AFTAC

Air Force Technical Applications Center

Design of Infrasonic Arrays

Robert R. Blandford
Directorate of Nuclear Treaty Monitoring

19980520 013

7 July 1997

Approved for public release.
Distribution Unlimited.

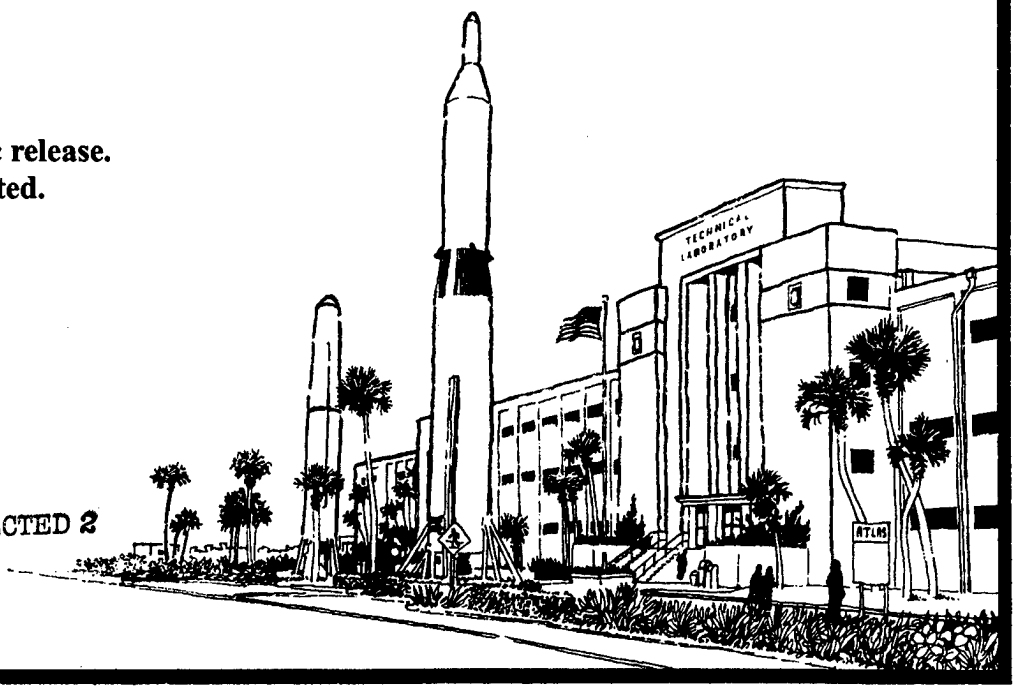

DTIC QUALITY INSPECTED 2

Report AFTAC-TR-97-013 has been reviewed and is approved for publication.

FRANK F. PILOTTE
Director of Nuclear Treaty Monitoring

JOHN T. WIGINGTON III
Colonel, USAF
Commander

Addressees: Please notify HQ AFTAC/TTR, 1030 S. Highway A1A, Patrick Air Force Base FL 32925-3002, if there is a change in your mailing address (including an individual no longer employed by your organization) or if your organization no longer wishes to be included in the distribution of future reports of this nature.

REPORT DOCUMENTATION PAGE

Form Approved
OMB No. 0704-0188

Public reporting burden for this collection of information is estimated to average 1 hour per response, including the time for reviewing instructions, searching existing data sources, gathering and maintaining the data needed, and completing and reviewing the collection of information. Send comments regarding this burden estimate or any other aspect of this collection of information, including suggestions for reducing this burden, to Washington Headquarters Services, Directorate for Information Operations and Reports, 1215 Jefferson David Highway, Suite 1204, Arlington, VA 22202-4302, and to the Office of Management and Budget, Paperwork Reduction Project (0704-0188), Washington, DC 20503.

1. AGENCY USE ONLY *(Leave blank)*	2. REPORT DATE	3. REPORT TYPE AND DATES COVERED
	7 July 1997	Technical

4. TITLE AND SUBTITLE
Design of Infrasonic Arrays

5. FUNDING NUMBERS

6. AUTHORS
Robert R. Blandford

7. PERFORMING ORGANIZATION NAME(S) AND ADDRESS(ES)
HQ Air Force Technical Applications Center (HQ AFTAC/TT)
1030 S. Highway A1A
Patrick AFB FL 32925-3002

8. PERFORMING ORGANIZATION REPORT NUMBER
AFTAC-TR-97-013

9. SPONSORING/MONITORING AGENCY NAME(S) AND ADDRESS(ES)

10. SPONSORING/MONITORING AGENCY REPORT NUMBER

11. SUPPLEMENTARY NOTES

12a. DISTRIBUTION/AVAILABILITY STATEMENT
Approved for public release. Distribution unlimited.

12b. DISTRIBUTION CODE

13. ABSTRACT *(Maximum 200 words)*

The Infrasound Experts Group of the Geneva Conference on Disarmament Ad Hoc Committee on a Nuclear Test Ban has recommended an infrasound array design consisting of four elements, with three elements forming an equilateral triangle and the fourth at the center of the triangle. The Experts recommended that the sides of the triangle be in the range 1 to 3 km.

In this report, in an attempt to place constraints on the array aperture, we evaluate the beamforming azimuthal estimation error of such arrays and compare it to historical data on observed azimuth residuals. The analysis for perfectly correlated signals shows that for beam signal-to-noise >> 1 the rms error is proportional to wavelength and inversely proportional to array aperture, beam amplitude signal-to-noise, and the square root of the time-bandwidth product. For beam signal-to-noise << 1 the relations are the same except that the rms error is inversely proportional to the *square* of the amplitude signal-to-noise.

(Continued on next page.)

14. SUBJECT TERMS		15. NUMBER OF PAGES
Infrasonic Arrays	Treaty Monitoring	44
		16. PRICE CODE

17. SECURITY CLASSIFICATION OF REPORT	18. SECURITY CLASSIFICATION OF THIS PAGE	19. SECURITY CLASSIFICATION OF ABSTRACT	20. LIMITATION OF ABSTRACT
UNCLASSIFIED	UNCLASSIFIED	UNCLASSIFIED	See Block 12a

Block 13 continued:

However, since data show that signals are not perfectly correlated, and that the signals become less correlated as the separation between sensors increases, a more complex analysis is needed in order to properly specify the type of array needed to achieve a desired azimuthal accuracy. For example, for a 5-second period signal, perfect correlation theory would lead to an estimated azimuth standard error 3.5 times smaller for an 8 km aperture array than would be predicted by the more accurate theory.

Using the more accurate theory, we find that for the 5-second period signal which is expected from a 1 kt atmospheric nuclear explosion, a 1 km aperture array at the detection threshold can have an azimuth estimation error, averaged over the signal duration, approximately equal to the best historically observed residual error. This observed error is shown to probably be true propagation error and not estimation error. At twice the detection amplitude threshold, or at 2-3 seconds period, the estimation error is substantially smaller than the propagation error.

Thus it may not be necessary to build arrays larger than 1 km in order that practical estimation errors be less than propagation errors for signals of interest. However, an array with a 2 km aperture, and including a central tripartite whose elements are separated by 200 km, would provide an array not so close to the margin and would give better performance at the higher frequencies which may be useful for regional monitoring and for source discrimination. In addition, the array may have significantly less aliasing at periods of interest and may therefore be able to better detect in the presence of interfering signals such as microbaroms.

In this report we use coherence values calculated from data from a large atmospheric nuclear test to parameterize the variance of the velocity and azimuth of infrasonic waves, and use these parameters to estimate the loss of signal coherence between two sensors as a function of signal period, distance between the sensors, and angle between the wavefront and the vector between the two sensors. We conclude that the loss of signal at 1 Hz for the 1 km array is 1.4 dB, probably acceptable, but for the 2 km array it is 3.8 dB, probably unacceptable if the array is to be used to monitor atmospheric events at regional distances. The addition of the 0.2 km aperture 3-element central array to the 2 km array overcomes this difficulty.

These conclusions are preliminary because the underlying data is available only for much larger periods and inter-sensor distances. Analysis of additional signal data at more appropriate periods and spacings is critically important.

CONTENTS

LIST OF FIGURES

LIST OF TABLES

ACKNOWLEDGMENT

Bob Shumway's theoretical analyses, printed in the Appendix and to be published elsewhere, forms the basis for the array design in this report.

ABSTRACT

The Infrasound Experts Group of the Geneva Conference on Disarmament Ad Hoc Committee on a Nuclear Test Ban has recommended an infrasound array design consisting of four elements, with three elements forming an equilateral triangle and the fourth at the center of the triangle. The Experts recommended that the sides of the triangle be in the range 1 to 3 km.

In this report, in an attempt to place constraints on the array aperture, we evaluate the beamforming azimuthal estimation error of such arrays and compare it to historical data on observed azimuth residuals. The analysis for perfectly correlated signals shows that for beam signal-to-noise >> 1 the rms error is proportional to wavelength and inversely proportional to array aperture, beam amplitude signal-to-noise, and the square root of the time-bandwidth product. For beam signal-to-noise << 1 the relations are the same except that the rms error is inversely proportional to the *square* of the amplitude signal-to-noise.

However, since data show that signals are not perfectly correlated, and that the signals become less correlated as the separation between sensors increases, a more complex analysis is needed in order to properly specify the type of array needed to achieve a desired azimuthal accuracy. For example, for a 5-second period signal, perfect correlation theory would lead to an estimated azimuth standard error 3.5 times smaller for an 8 km aperture array than would be predicted by the more accurate theory.

Using the more accurate theory, we find that for the 5-second period signal which is expected from a 1 kt atmospheric nuclear explosion, a 1 km aperture array at the detection threshold can have an azimuth estimation error, averaged over the signal duration, approximately equal to the best historically observed residual error. This observed error is shown to probably be true propagation error and not estimation error. At twice the detection amplitude threshold, or at 2-3 seconds period, the estimation error is substantially smaller than the propagation error.

Thus it may not be necessary to build arrays larger than 1 km in order that practical estimation errors be less than propagation errors for signals of interest. However, an array with a 2 km aperture, and including a central tripartite whose elements are separated by 200 km, would provide an array not so close to the margin and would give better performance at the higher frequencies which may be useful for regional monitoring and for source discrimination. In addition, the array may have significantly less aliasing at periods of interest and may therefore be able to better detect in the presence of interfering signals such as microbaroms.

In this report we use coherence values calculated from data from a large atmospheric nuclear test to parameterize the variance of the velocity and azimuth of infrasonic waves, and use these parameters to estimate the loss of signal coherence between two sensors as a function of signal period, distance between the sensors, and angle between the wavefront and the vector between the two sensors. We conclude that the loss of signal at 1 Hz for the 1 km array is 1.4 dB, probably acceptable, but for the 2 km array it is 3.8 dB, probably unacceptable if the array is to be used to monitor atmospheric events at regional distances. The addition of the 0.2 km aperture 3-element central array to the 2 km array overcomes this difficulty.

These conclusions are preliminary because the underlying data is available only for much larger periods and inter-sensor distances. Analysis of additional signal data at more appropriate periods and spacings is critically important.

INTRODUCTION

Design of an infrasound array presents a classic problem in array design: the trade-off between signal-to-noise and location accuracy. Although infrasonic noise becomes uncorrelated at all periods at distances of less than 100 meters (McDonald et al., 1971; Blandford and Clauter, 1996), the signals themselves become substantially uncorrelated only at distances ranging from 1 to 50 kilometers (km) for periods ranging from 1 to 50 seconds (Mack and Flinn, 1971).

Thus, for a fixed number of sensors, as array aperture increases beyond a few hundred meters, the signal-to-noise ratio decreases. However, it seems intuitively clear that if the signal does not become too uncorrelated, the increased aperture will enable a more accurate estimate of the signal's arrival azimuth and slowness.

It is commonly thought that the location capability of an array is a fixed number given by, for example, the width of the 3-decibel (dB) point in the array response. However, a moment's reflection will show that this cannot be strictly correct. If the signal-to-noise is sufficiently poor then no location capability exists. And, perhaps more difficult to see, if the signal-to-noise is arbitrarily high then the location precision also can be arbitrarily good. One need only climb to the very peak of the wavenumber response of the signal. For perfect signal correlation Harris (1990) has shown, for example, that for a fixed-sized array the root-mean-square (rms) slowness error is inversely proportional to the amplitude signal-to-noise ratio and also inversely proportional to the square root of the time-bandwidth product of the signal.

Now, when several repetitions of an azimuthal estimate are made with a fixed signal-to-noise, one expects some standard error of the estimates, and one expects that this error will depend on the signal-to-noise. Wu (1982) derived a formula for this standard error using a statistical analysis assuming perfect correlation of fixed but unknown signals. Harris (1990) also gave azimuth error estimates for beamforming of fixed, unknown signals.

The formulas used in this report are quite similar for perfectly correlated signals and are derived in the Appendix which is authored by R. Shumway. However, in this report we assume not that the signals are fixed and unknown, but that they are stochastic with known spectrum. Also in the Appendix is the analysis for stochastic signals which are not perfectly correlated.

Of particular interest is the performance of arrays designed as recommended by the Infrasound Experts Group of the Geneva Conference on Disarmament (CD) Ad Hoc Committee on a Nuclear Test Ban as found in Working Paper 224 (1995). This design comprises a 4-element array with three of the elements arranged in an equilateral triangle and the fourth element in the center. The spacing between the outer three elements is yet to be determined, but was suggested by the Experts to be between 1 and 3 km depending on the detection range and on the details of the signal processing algorithms.

McKisic (1996), drawing on reports by Olmstead (1952), presents data showing that the dominant period of signals observed from 1.2 kiloton (kt) atmospheric nuclear explosions at distances between 1000 and 3600 km ranged from the 3- to 10-second period, with modes at 4-6 seconds. Since these distances are typical of the closest distances that can be expected between an event

and the stations in the 60-station infrasound network suggested in Working Paper 224 (1995), it would appear that the array design should be optimized for these periods.

Note, however, that it may be useful for arrays to have good signal-to-noise at other periods, both shorter and longer, if these may be used for discrimination between air nuclear blasts and other sources such as bolides or mining blasts. The shorter periods, as might be expected, and as we shall see, also offer the possibility of better precision in azimuth estimation.

A classical approach to detection involves beamforming the traces of an array, performing a short-term over long-term amplitude ratio, and selecting the beam with the maximum ratio as the beam directed toward the source. The peak of the beam power is used to determine the azimuth to the event. The Appendix shows that this procedure is actually the optimum azimuth estimator for the case of perfectly correlated signals, and that a form of weighted beamforming is optimum in the case of imperfectly correlated signals.

It is worth noting that, in the presence of non-stationary noise, it would be useful to estimate the noise in the signal window. This would lead to estimating the azimuth by the peak of the F statistic, given by the ratio of the signal power to the noise power, in place of the peak of the signal power alone. Also, in the case where noise levels vary strongly between channels of the array, a generalized F statistic may be computed in which each channel's contribution to the signal estimate is weighted by the estimated noise on the channel (Shumway (1996), personal communication). In practice, this is the case for infrasound and so future development of advanced detectors and estimators along these lines is desirable.

There are other detection and location processors possible, for example, the correlator detector referenced by Cook and Bedard (1971). This detector computes the maximum cross-correlation between all pairs of channels and detects on the average of these maxima. Then the azimuth may be determined by fitting a plane wave to the delays determined by the cross-correlation maxima. However, in contrast to the analysis in this report, there is no available statistical time series analysis of the correlation detector and locator, and so we cannot yet quantitatively estimate the variance of its performance as a function of array aperture and signal correlation. However, classical statistical estimation theory would lead us to expect that beamforming would be the optimum processor so that correlation processors could perform no better.

THEORY

Beam Loss

When an array of N sensors is beamformed, and the noise is correlated, then the noise on the beam is reduced according to the form:

$$dB = \log 10[N/(1+(N-1)\rho)] \quad (1)$$

where ρ is the average noise cross-correlation between pairs of the N traces considered (Blandford and Clark, 1975). A similar formula holds for loss of signal due to lack of correlation between signals if the correlation is less than unity.

Representation for Empirical Infrasonic Signal Coherence

Mack and Flinn (1971) analyzed infrasound records from the December 27, 1968, Chinese atmospheric nuclear test as recorded at the 13 microbarographs of the Large Aperture Microbarograph Array (LAMA). This array had an aperture of approximately 60 km and the microbarographs were coincident with the center elements of subarrays of the corresponding seismic array, LASA. The closest elements of the infrasound array were 7 km apart, and the periods analyzed ranged from 10.7 to 85.7 seconds. Mack and Flinn (1971) computed the coherence between pairs of microbarographs and showed that the loss of coherence was greater for sensors oriented parallel to the wavefront than for those oriented perpendicular to the wavefront.

Mack and Flinn (1971) used a signal model in which the signal was described by a uniform distribution of waves within an azimuth/velocity window in frequency wavenumber space. They fitted the coherence data with an equation of the form:

$$\gamma^2 = \left|\frac{\sin(2\pi k_o x \sin\Delta\theta)}{2\pi k_o \sin\Delta\theta}\right|^2 \cdot \left|\frac{\sin(2\pi\Delta k y)}{2\pi\Delta k y}\right|^2 \quad (2)$$

In this expression the wavenumber $k = 1/\lambda$ where the wavelength λ=c/T where c is the phase velocity (approximately 0.3 km/sec for infrasound) and T is the period in seconds. Mack and Flinn (1971) determined that a suitable value for $\Delta\theta$ was 5° and for Δk, values were calculated for different values of T corresponding to Δc=0.015 km/sec. This latter value is greater than that for the theoretical curves plotted in most of the figures in Mack and Flinn (1971), however, we may see that their data most relevant to this study, that plotted in their Figures 6 and 14 for T=10.7 seconds, falls below their curve for Δc=0.010 km/sec. Therefore in this paper we use Δc=0.015 km/sec.

In the results section to follow we must keep in mind that the above azimuth and wavenumber variances were determined for 10- to 85-second periods and 7- to 60-km element spacings. They are, however, at the most extreme, applied to 0.5-second periods and to 0.2-km spacings. Only if the model of propagating waves is also correct at these periods is it likely that the extrapolation of the data taken at the different periods and spacings will be valid. It is critical that further evaluation of good signal-to-noise data at the shorter periods and spacings be carried out.

For comparison with future observations Figure 1 and Table 1 give the predicted values from the

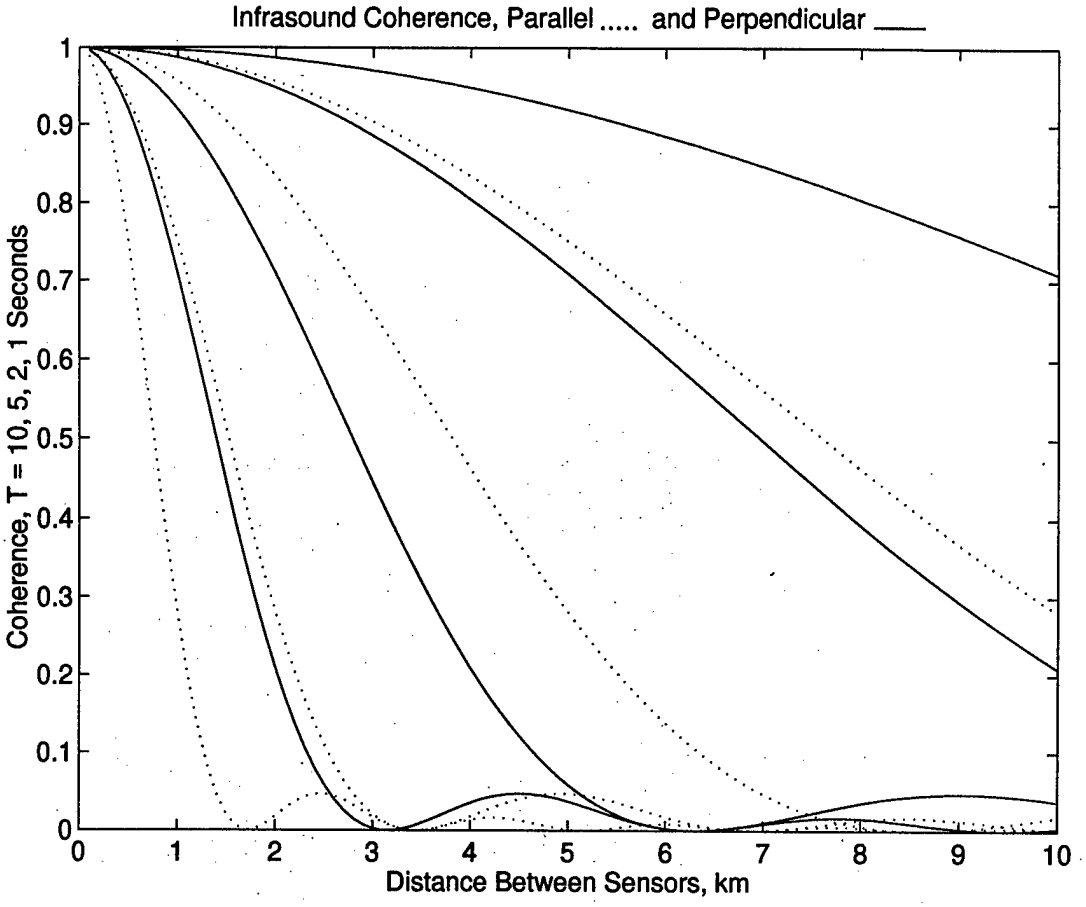

Figure 1. Coherence as a function of intersensor distance for T=10, 5, 2, 1 seconds according to equation (2) using Δc=0.015 km/sec and $\Delta\theta$=5 degrees as determined from Mack and Flinn (1971), parallel and perpendicular to the wavefront.

preceding equation for infrasound coherence as a function of period, *d*, distance between sensors, and direction of approach with respect to the wavefront.

The periodic behavior of the coherence at low values of coherence for the larger distances as seen in Figure 1 is not reflected in the original data and is simply an artifact of the form of the functions in (2) used to fit the observed data.

The low values of coherence seen at 8-km spacing for 2-1 Hertz (Hz) seem to conflict qualitatively with a signal seen at AFTAC arrays, so there is reason to suspect that the coherence values used in this report are too small and thus that conclusions for short periods and large apertures are overly pessimistic. On the other hand, calculations using (2) for spacings of 0.1 km, a typical value for Department of Energy (DOE) arrays, gives coherence values between 0.99 and 0.83 for 1-4 Hz, in agreement with qualitative observations for those arrays.

The preceding analytical expression for coherence is, for frequency-filtered, aligned, identical signals in the time-domain which have been randomly perturbed, equal to the correlation and so we shall treat it in this report as equal to ρ in the signal loss equation, (1).

Period (sec)				
1	2	5	d (km)	
0.71	0.92	0.99	1	sensors
0.21	0.71	0.95	2	perpendicular
0	0.44	0.88	3	to
0	0.21	0.80	4	wavefront
0	0.04	0.39	8	
0.28	0.75	0.96	1	
0.02	0.28	0.83	2	sensors
0	0.02	0.66	3	parallel
0	0.02	0.46	4	to
0	0	0.01	8	wavefront

Table 1: Predicted Coherence from Equation (2)

Implications of Coherence Variation with Frequency and Distance

The behavior of coherence as plotted in Figure 1 has immediate implications for array design. We note that, for both parallel and perpendicular waves, for 5-second waves the coherence is greater than 0.95, 0.8, and 0.65 at 1, 2, and 3 km, respectively. These values are likely great enough to ensure that almost any processing technique which relies on coherence will work satisfactorily for the CD arrays whose intersensor spacings are equal to the array side and 0.577 times the array side.

On the other hand, for 1 Hz we see that the coherence is between 0.7 and 0.25 at 1 km, but is only between 0.2-0.02 and 0.0 and 0.02 at 2 and 3 km, respectively.

The 1-km array appears to have adequate coherence at 1 Hz; but for the 2- and 3-km side arrays, coherence processing between the outer elements will be useless. For the 3-km array the closest spacing is 1.73 km for which the coherence varies between 0.35 and 0.0. These values cast doubt on the robustness of any processor, such as all suggested detection processors, for the 3-km arrays which relies on the coherence of 1 Hz signals.

At 2 km the minimum spacing is 1.15 km which has coherence at 1 Hz between 0.6 and 0.15. It is not clear how robust an array processor can be with such coherence values for three intersensor spacings, and values between 0.2 and 0.02 for the other three.

Thus, general considerations of coherence suggest that if it is desired to detect 1 Hz signals, CD arrays with apertures larger than 1 km are not likely to be satisfactory.

Azimuth Standard Error for Perfectly Correlated Signals

In the Appendix, equation (39) gives an expression for the mean square azimuthal error for an array with perfect signal coherence, given the covariance matrix of the array coordinates. For all of the arrays considered in this report, the correlation between the array element locations, which would otherwise figure in the expanded equation, is zero and $\sigma_x = \sigma_y = \sigma$. In this case, the equation may be greatly simplified so that the physical parameters controlling the error are more clearly revealed, and the result is seen as equation (3).

$$\sigma_a = \left(\frac{180}{\pi}\right)\cdot\left(\frac{1}{2\pi}\right)\cdot\left(\frac{1}{2BT}\right)^{\frac{1}{2}}\cdot\left(\frac{1}{N\cdot snr}\right)^{\frac{1}{2}}\left(1+\frac{1}{N\cdot snr}\right)^{\frac{1}{2}}\left(\frac{\lambda}{\sigma}\right) \qquad (3)$$

In this equation, N is the number of sensors in the array, σ is the square root of the diagonal covariance matrix element of the array coordinate, and *snr* is the theoretical power signal-to-noise ratio on a single element of the array; σ_a is expressed in degrees rather than radians.

We see that the azimuthal error is independent of the direction of approach and is directly proportional to the signal wavelength, inversely proportional to the array aperture, and, for high signal-to-noise, inversely proportional to $(N\cdot snr)^{1/2}$. In the case of uncorrelated noise and for a perfectly correlated signal, this is equal to the beam amplitude signal-to-noise ratio.

It is worth noting that the term$(1 + 1/(N\cdot snr))^{1/2}$ seen in (3) is not present in the theory of Wu (1982) which otherwise results in a formula identical to (3). The difference is apparently due to the differing statistical assumptions in the two studies. Wu (1982) assumes that the signal is fixed but unknown, the present study assumes, in order to appropriately treat the incoherent case, that the signals are stochastic. In the limit of perfect correlation one might expect that the stochastic signal would give the same result as fixed-identical but unknown signals, but apparently there is this one-term difference.

The effect of this additional term is, for low signal-to-noise, to make the error increase in inverse proportion to the beam *power* signal-to-noise instead of inversely to the beam *amplitude* signal-to-noise. In addition, at the threshold of detection where the beam signal-to-noise is near unity, the azimuthal variance for the stochastic case is approximately doubled by the additional term.

Note also that the azimuth error is inversely proportional to the square-root of the time-bandwidth product, *BT*, of the time window analyzed. It is this term which is responsible for reducing the azimuth variance when several azimuth estimates from a long train of arrival pulses are averaged together.

Azimuth Standard Error for Less-Than-Perfect Correlation

Although the theory for perfect correlation offers some physical insight, we shall see that it is inadequate for designing infrasonic arrays where, for apertures and signal periods of interest, the lack of signal correlation strongly affects the azimuth estimation precision. In the Appendix, the relevant equation is equation (46) which may be transformed to the form:

$$\sigma_a = \left(\frac{180}{\pi}\right)\cdot\left(\frac{1}{2\pi}\right)\cdot\left(\frac{1}{2BT}\right)^{\frac{1}{2}}\cdot\left(\frac{1}{N\cdot snr}\right)^{\frac{1}{2}}(\lambda^2)(2N)^{\frac{1}{2}}(\tilde{\theta}'\cdot D_P^{-1}\cdot\tilde{\theta})^{\frac{1}{2}} \qquad (4)$$

where $\tilde{\theta}$ is related to the estimated signal wavenumber components k_x and k_y by $\tilde{\theta} = (k_y,-k_x)'$. (Note the reverse placement of the vector components; the prime mark indicates the transpose operation.) D_P is given by $D_P = P_s^{-1}\cdot D$ where P_s is the power spectrum, assumed in this application, although not in the Appendix, to be the same at each sensor, and D is the 4x4 matrix which is the generalization of the array element location covariance matrix, and is given by equation (42) in the Appendix as

$$D = \sum_{j,k} c_{jk}\cdot F^s_{kj}\cdot(\vec{r}_j-\vec{r}_k)\cdot(\vec{r}_j-\vec{r}_k)' \qquad (5)$$

where $\vec{r}$ are element coordinates, and $F^s_{kj} = P_s^{-1}\cdot f^s_{kj}$ where f^s_{kj} is the signal covariance matrix.

In this application the off-diagonal elements of F^s_{kj} are given by the coherence, given by (2).

The signal-to-noise enters the calculation of D through the relation for the matrix for c_{jk}

$$C = F_s\cdot\left(F_s+\frac{1}{snr}\cdot I\right)^{-1}$$

It does not appear possible to write (5) in pure matrix notation.

RESULTS

CD Array Geometry

For an array in the form of an equilateral triangle, 1 km on a side with a fourth instrument at the center, the array of (x, y) coordinates is:

x (km)	y (km)
0.0	0.0
0.0	0.577
0.5	-0.289
-0.5	-0.289

Table 2: CD Infrasound 1 Km Array, Nominal Coordinates

For an array of this shape with a side of 3 km instead of 1 km all of these dimensions would, of course, be multiplied by 3.

For the array in Table 2, the covariance matrix, with *N* as the denominator instead of the usual *N-1*, is:

0.125	0.0
0.0	0.125

Table 3: CD Infrasound 1 Km Array Covariance Matrix

For an array with sides 3 km long, the elements in this matrix would be 9 times as large. The parameter σ, which is $(0.125)^{1/2} = 0.35$ would be 3 times as large for a 3-km array.

Signal Parameters

The value of *snr* chosen for most tabulations in this report is $(0.75)^2$ since for a 4-element array, assuming perfect signal correlation and uncorrelated noise, this will lead to an amplitude signal-to-noise on the beam of 1.5. This value of signal-to-noise is the traditional value accepted as sufficient for a seismic analyst to confidently declare a detection; and examination of infrasound signals in noise reveals many qualitative features in common with seismic signals, e.g., a relatively broadband and pulse-like character, so that use of this value for *snr* seems reasonable.

Plots of signals from a few kilotons of conventional explosives detected at distances of a few thousand kilometers have been published by Whitaker et al. (1990). These waveforms are characterized by about six pulses of energy; with the duration of each pulse about 60 seconds. Thus we shall choose T = 60 seconds for our calculations. The bandwidths tabulated are centered on T= [20, 10, 5, 2, 1, 0.5] seconds and the bandwidths are simply taken from the center-points of the

adjacent bands (thus the bands overlap), with the additional parameters of 40 seconds and 3 Hz for the lower and upper limits for the lower and upper bands. The BT product is between 1.0 and 2.0 for all bands. All calculations presented are for an azimuth of approach of 30 degrees East of North. Test calculations for other directions differed insignificantly.

Because of the likely operational procedure of averaging over perhaps four of the 60-second windows, it should be kept in mind that most tabulated standard errors, which are for a single 60-second window, could be reduced by a factor of two.

In evaluating an infrasonic array we must consider both the detection and location capability. Therefore, we shall tabulate two parameters, signal loss and azimuth error, as a function of array aperture and signal period.

Beam Signal Loss

Table 4 gives the beam signal loss in accordance with equation (1). We see that for larger arrays and for shorter periods there is substantial signal loss. If detection and estimation were based on simple beamforming, one would expect large losses in capability. However, we have seen that in the case of loss of coherence the optimum processor is a weighted beam.

	Period (sec)/Bandwidth (Hz)					
d (km)	20/0.075	10/0.15	5/0.4	2/0.8	1/1.5	0.5/2
1	0.00	0.01	0.06	0.38	1.4	3.8
2	0.02	0.06	0.24	1.4	3.8	5.7
3	0.03	0.14	0.54	2.7	5.2	6.0
4	0.06	0.24	0.93	3.7	5.7	6.0
8	0.24	1.0	2.9	5.7	6.0	6.0

Table 4: Beam Signal Loss (dB), 4-Element CD Array, d km on a Side According to Equation (1).

In agreement with the discussion given previously of Figure 1, we see that there is a signal loss of 3.8 and 5.2 dB for detection at 1-second for 2 and 3 km aperture arrays. This suggests that most detectors will perform poorly for such apertures. In particular, one would suspect that detectors which depend on correlation between signals, such as infrasound detectors, would perform poorly.

It should be noted that in the case of infrasound detection the detection and estimation statistic would be not the beam power divided by the long-term noise, but is instead the beam power divided by the residual noise estimated during the signal window. This latter statistic has an F distribution and is, therefore, commonly referred to as an "F detector." F-type detectors are used in infrasound detection because of the presence in infrasound data of uncorrelated noise bursts due to cells of low pressure advected by the local wind.

Comparison of Azimuth Precision for Perfectly Correlated and for Uncorrelated Signals

Table 5 gives the azimuth estimate error both for perfect coherence and for coherence in accordance with equation (2). We see that the effect on azimuth error of the loss of signal coherence is substantial. While values as low as 0.02 degrees are seen for perfect coherence, and it is clear that in theory increasing the aperture of the array and the frequency of the signal will lead to arbitrarily good precision, in practice the best accuracy obtained for the imperfect correlation case is 30 times larger: 0.65 degrees; and it occurs for the shortest period for the smallest array.

	Period (sec)/Bandwidth (Hz)					
d (km)	20/0.075	10/0.15	5/0.4	2/0.8	1/1.5	0.5/2
1	41.3/41.4	14.6/14.7	4.5/4.5	1.26/1.39	0.46/0.66	0.20/0.65
2	20.6/20.7	7.3/7.4	2.2/2.4	0.63/0.90	0.23/0.75	0.10/2.87
3	13.7/13.9	4.9/5.0	1.39/1.71	0.42/0.86	0.15/1.49	0.07/33.6
4	10.3/10.5	3.6/3.9	1.12/1.42	0.32/1.02	0.12/3.31	0.05/3.95
8	5.2/5.5	1.8/2.3	0.56/1.25	0.15/4.54	0.06/4.56	0.02/117

Table 5: Azimuth Error (deg), 4-Element CD Array, d km on a Side Single-Element Amplitude Signal-to-Noise of 0.75. Perfect signal correlation according to equation (3) and imperfect correlation according to (4). Variability at the bottom of last column reflects low-coherence details of equation (2). As mentioned in the text, values seen here should be reduced by a factor of at least 2 to account for the signal character in which several 60-second pulses are spread out over time.

Qualitative Discussion of Azimuth Precision for Uncorrelated Signals

Note that this most precise azimuth estimate for realistic coherence occurs at values of period and aperture where the signal loss is 3.8 dB out of a possible 6 dB (Table 4) and where, therefore, the coherence is much smaller than unity. Thus, there is a complex calculation required to determine the generalized beam to be maximized to determine this azimuth, as seen from the discussion of equation (40) in the Appendix. Determining this generalized beam requires a good estimate of the array coherence. Thus, improved estimates at higher frequencies and larger apertures may come at the expense of extra analysis and processing, reducing the advantage from a system point of view of the larger aperture arrays.

From a qualitative point of view we see, for example, for the 2 km aperture array, that there is a minimum standard error, 0.75 degrees, as a function of period at 1-second period. The increase in error toward longer periods reflects a lessening of the relative array aperture, while going toward shorter periods the increase in error reflects a loss in signal coherence.

Another point of interest is the erratic values in lower rows of the last column of Table 5. These presumably reflect the low-amplitude oscillations of the coherence at large sensor spacings and short periods and, as discussed previously, are an artifact of the curve-fitting procedure. One can only be sure that the error is large for these apertures and periods.

A important point is that the standard detectors now being investigated for infrasound arrays would be less likely to work well at shorter periods and larger apertures because they rely on signal correlation.

Estimate of Standard Error of Azimuth Due to Propagation Error

We also see from Table 5 that the CD array with an aperture of 1 km would have a standard error of azimuth estimation of 4.5 degrees at 5-second period for a threshold detection. This value is greater than the 1.8 degree rms azimuth standard error determined by the 7-11 km aperture AFTAC arrays for the distance range 0 to 2000 km (Blandford and Clauter, 1996). Table 5 also shows, assuming an 8 km aperture, that the AFTAC arrays would have had a threshold azimuth error approximately of 1.25 degrees at 5-second period.

However, it is important to realize that the AFTAC azimuth estimates were likely obtained at substantially better than threshold signal-to-noise ratios, that the azimuths were averaged over several successive windows, and that signals of shorter periods than 5 seconds were sometimes used.

Calculations using equation (3) shows that for an 8 km aperture array, the azimuth resolution for a sensor amplitude signal-to-noise of 3.0, perhaps more typical for AFTAC experience, the azimuth resolution would be 0.48 degrees, much less than the 1.8 degrees observed.

In addition, as mentioned previously, were the azimuths averaged over four successive 60-second arrival windows, the average azimuth precision would be improved by an independent factor of 2.

Thus, it seems reasonable that the precision achievable in the early AFTAC arrays would have been better than the 1.8 degrees observed, suggesting that this standard error estimate is of propagation error rather than measurement error.

As an historical note, Table 5 suggests that periods shorter than 5-second period would not be as useful for azimuth determination for a 4-element array with an 8 km aperture. However, the range of models over which the likelihood is maximized in the Appendix does not include techniques which take advantage of delays between signal *onset* at different sensors. It may be that higher frequencies can be used in some such incoherent processing method, resulting in better precision than indicated for shorter periods in Table 5.

Implications for Array Aperture

The implication of the foregoing section is that precision better than 1.8 degrees would not be needed in the CD network because it would comprise only a small fraction of the total variance which includes the natural variance due to propagation. This raises the question of whether a 1 km aperture array could be satisfactory or whether it would be useful to increase the array aperture to 2 or 3 km where the azimuthal error at the detection threshold is seen in Table 5 to be improved from 4.54 degrees to 2.38 and 1.71 degrees, respectively.

We must first consider that many signals will be received at better than the threshold detection level resulting in better azimuth estimate precision. For example, if the amplitude signal-to-noise on the beam was 3.0 instead of 1.5, the azimuth error for the 1 km array may be calculated to be 2.01 degrees instead of 4.54.

In addition, one must consider that the azimuth estimate may be averaged over, for example, four different 60-second windows. In this case, also, the azimuth error would be reduced by a factor of 2. Now one might well expect that this would be standard practice so that it seems reasonable to assume that the precision attainable in a 1-km aperture array would be better than 2.27 degrees even at the threshold, and at signal-to-noise of 3.0 the precision would be 1.0 degrees.

Finally, note that, even at the threshold and with no averaging over several windows, the precision for the 1-km array at 2 seconds period is 1.39 degrees, and at 1-second it is 0.66 degrees. The precision at these shorter periods may be seen in Table 5 to be substantially the same for the 2-km aperture and it is likely to be critical to use the coherence-weighted beam to attain these results for the larger array; notice in Table 4 that there is a 3.8 dB beam loss at 1 Hz for the 2 km array.

Thus, it seems that a 1-km aperture array has an azimuth estimation capability that is very close to good enough that location capability will not suffer for 1-kt events at distances less than 2000 km. (At larger distances the propagation error is much larger than 1.8 degrees, so that a 1-km aperture array is surely adequate.) Furthermore, the processing required at the smaller apertures is likely to be simpler. However, let us remember that these conclusions at 5-second period and 1-km spacing are based on model extrapolation from data taken at 10.7 seconds period and 7-km spacing. As mentioned earlier, analysis of more relevant data is crucial.

From another angle, let us consider the loss in signal coherence as one increases the aperture above 1 km. As seen in Table 4, while the signal loss is negligible at T = 5 seconds, it is 3.8 dB at 0.5-second period for 1-km aperture, and as just noted, 3.8 dB even at 1 Hz for 2-km spacing.

Recent work in the analysis of underground and surface mining blasts by use of infrasound arrays suggests that much useful information for treaty monitoring might be garnered at these frequencies if infrasound arrays were within a few hundreds of kilometers of the mine (E. Herrin, personal communication). In order to retain the capability of analyzing these events, it seems imprudent to increase the array aperture above 1 km.

Designs with an Additional 3-Element Subarray

To improve the long-period location capability without further degrading the high frequency performance, one could add a small central tripartite. Table 6 shows nominal coordinates for the base 1-km aperture array to which one adds an additional three elements as an inverted equilateral triangle with sides of 0.2 km at the center of the CD array; Tables 7 and 8 show the resulting signal loss and azimuth precision.

x (km)	y (km)
0.0	0.0
0.0	0.577
0.5	-0.289
-0.5	-0.289
-0.1	0.0578
0.1	0.0578
0.0	-0.115

Table 6: CD 1-km Aperture Array Plus Central Subarray 0.2 km on a Side

In Table 7 we see that, indeed, for 1 km, this array loses only 0.6 dB at 0.5 seconds, relative to a 4-element array with perfect signal correlation. At 2-km aperture we see only a loss of 1.6 dB. Thus, this array should have a better detection threshold than the 4-element array at all periods and should be much more capable at short periods, including those less than 0.5 seconds.

	Period (sec)/Bandwidth (Hz)					
d (km)	20/0.075	10/0.15	5/0.4	2/0.8	1/1.5	0.5/2
1	-2.4	-2.4	-2.4	-2.2	-1.6	0.6
2	-2.4	-2.4	-2.3	-1.6	0.0	1.6
3	-2.4	-2.3	-2.1	-0.8	1.1	1.9
4	-2.4	-2.3	-1.9	-0.1	1.5	1.8
8	-2.3	-1.9	-0.7	1.5	1.7	1.9

Table 7: Beam Signal Loss (dB), 7-Element Array Consisting of a CD Array, *d* km on a Side, Plus an 0.2 km on a Side, Inverted Centered Equilateral Triangle. Beam signal loss relative to a 4-element array with perfect signal correlation. Negative loss indicates a gain in beam signal-to-noise. The slight non-monotonic element in the 0.5-second column reflects slight changes in mean signal correlation as changing array proportions bring different proportions of station pairs parallel and perpendicular to the wavefront (see Figure 2).

By comparing Tables 8 and 4 we see that there is little improvement in azimuth error for periods greater than 1 second. However, for 1-second period and greater the gains are substantial. In general terms it is clear that the addition of the subarray has stabilized the performance of the arrays

as a function of frequency. For all apertures and for periods of 5 seconds or less, we see fairly uniform performance with azimuth error roughly in the range 0.5 to 2.0 degrees. One suspects that this stability will be reflected in robust behavior of processing algorithms.

	Period (sec)/Bandwidth (Hz)					
d (km)	20/0.075	10/0.15	5/0.4	2/0.8	1/1.5	0.5/2
1	37.8	13.4	4.1	1.25	0.56	0.44
2	19.2	6.9	2.2	0.78	0.55	0.94
3	12.9	4.7	1.6	0.70	0.94	1.06
4	9.7	3.6	1.3	0.77	1.8	1.03
8	5.1	2.1	1.0	3.4	2.1	1.06

Table 8: Azimuth Error (deg), 7-Element Array, CD Array, *d* km on a Side, Plus an 0.2-km on a Side, Inverted Centered Equilateral Triangle. Single-element amplitude signal-to-noise of 0.75. Calculated for non-perfect correlation using equation (4).

QUALITATIVE BEHAVIOR

Figure 2 shows the decrease in azimuthal error as a function of signal-to-noise for a period of 5 seconds for the 4-element, 1- and 2-km aperture arrays and for the 2-km, 7-element array. Evaluations for signal-to-noise at 10, 100, and 1000 shows that the asymptote for large signal-to-noise is approximately 0.3. This shows that one eventually reaches the point where the azimuth precision is limited by the loss of signal coherence and cannot be improved further. We further see that for this period the 2-km arrays have a substantial advantage over the 1-km array, but that there is little advantage to adding the small subarray.

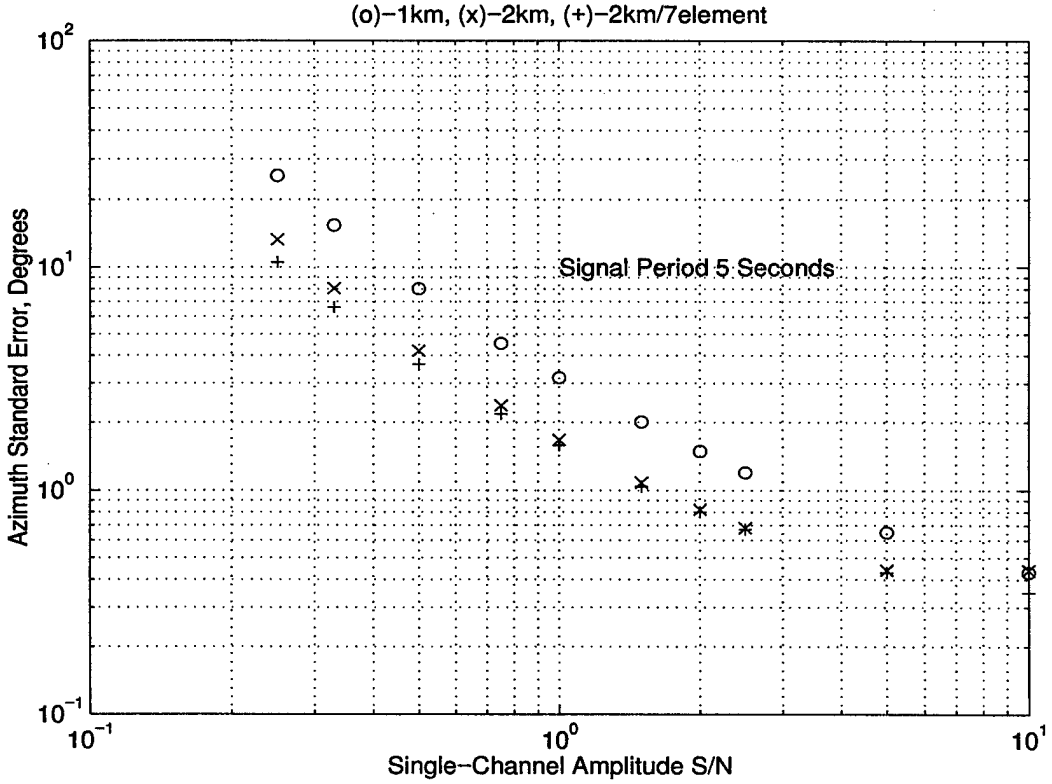

Figure 2. Azimuthal error as a function of signal-to-noise for a signal period of 5 seconds for the 4-element, 1- and 2-km aperture arrays and for the 2-km, 7-element array; from equation (4).

Figure 3, in comparison to Figure 2, shows that for a signal period of 1 second the absolute error is substantially less than for a signal period of 5 seconds. In this case, all arrays are rather close in capability although the 2-km, 7-sensor array is always the best or very close to the best. The only exception is for signal-to-noise between 2 and 3 where the 1-km aperture array is slightly better. In general the 2-km aperture array is a factor of 1.5 to 2.0 worse than the others.

It is important to realize that the fairly good performance of the 2-km, 4-element array at 1-second period comes only at the expense of complex optimum processing, as expressed, for example, in equation (41) in the Appendix, requiring substantially more work than simple beamforming or cross-correlation. In addition, these processes have never been executed in practice.

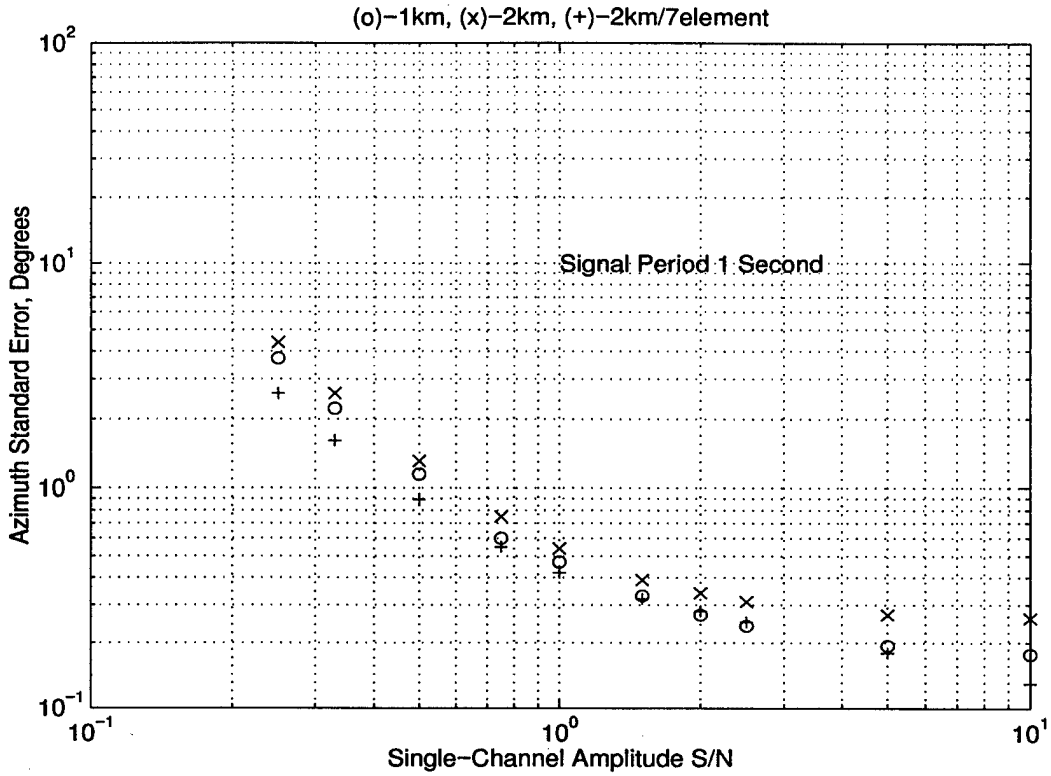

Figure 3. Azimuthal error as a function of signal-to-noise for a signal period of 1 seconds for the 4-element 1 and 2 km aperture arrays and for the 2 km, 7-element array. From equation (4).

In Figure 4, at the top of the next page, we compare the azimuth estimation of these arrays as a function of signal period. We see that the small array behaves relatively poorly at the long periods and that the 4-element, 2-km array "blow up" at 0.5 seconds period as is reasonable due to the loss of coherence and the absence of a closely-spaced subarray.

In Figure 5, at the bottom of the next page, we see how at the azimuth estimation capability varies with azimuth for the 4-element and 7-element arrays. At 5-second period we see that the capability improves (azimuth error declines) as the aperture increases, while the 1 Hz capability becomes worse. However, as the aperture becomes quite large, the 7-element array performs much better than the 4-element array.

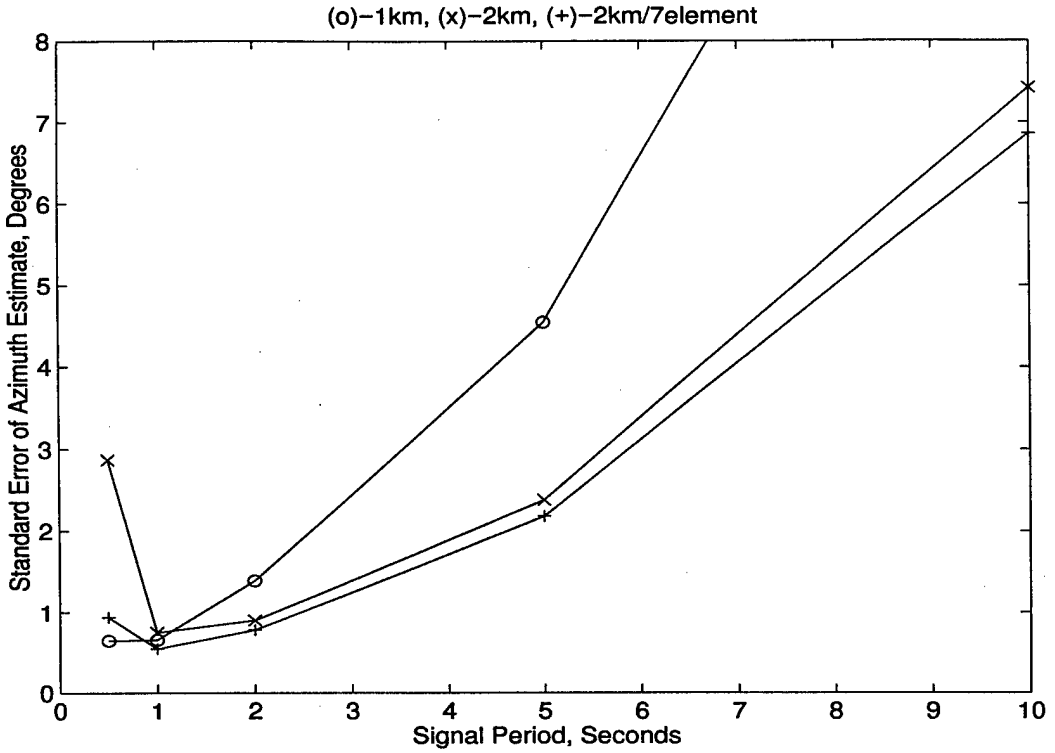

Figure 4. Comparison of Azimuthal Estimation as a Function of Signal Period.

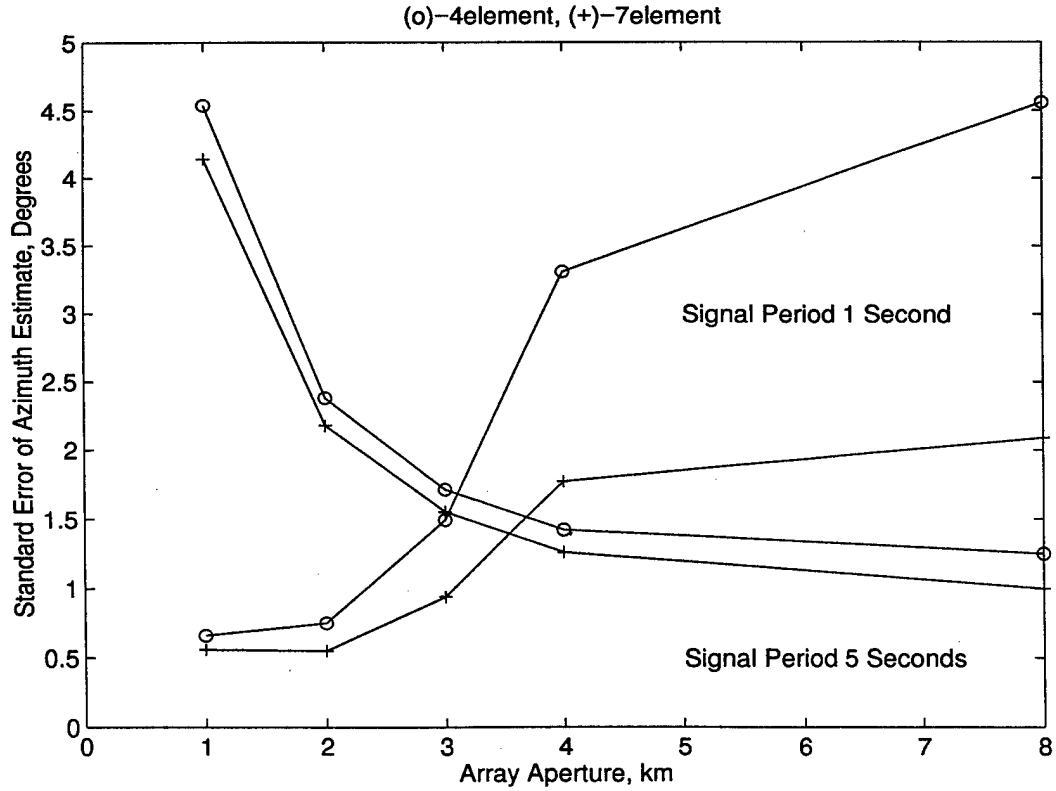

Figure 5. Azimuthal Estimation Capability.

SUMMARY

Based on data available to date, the 4-element CD infrasonic arrays should be built with an aperture of approximately 1 km. Loss of signal correlation for the 5-second signals expected from 1 kt explosions at distances of 2000 km are expected to be small enough so that detection using standard detection techniques will be unaffected. The expected azimuth estimation error at the detection threshold for a 5-second period signal series of four 60-second pulses, as expected from a 1 kt explosion at a distance of 2000 km, is approximately the same as the 1.8 degree variation of true azimuth of arrival from the true back azimuth to the source due to propagation at these distances.

Since the azimuth estimation error is inversely proportional to the beam amplitude signal-to-noise, and also inversely to the square root of the signal duration and bandwidth, we have seen that it is very likely that the azimuth to most real 1 kt signals will be calculated to a precision substantially smaller than the natural variation.

The 1 km aperture array has only 1.4 dB loss at 1-second period, but has a 3.8 dB loss at 0.5 second period. Should this be thought excessive for any required analysis of nearby mining explosions (not likely a consideration at remote stations in the Southern Hemisphere, but very possibly a consideration in inhabited areas) then it might be useful to install a small, perhaps 0.2-km aperture, 3-element subarray. The small subarray enhances detection of long period signals and reduces the array loss at short periods. It does not significantly change the location capability of the 1-km array, but would make it possible to expand that array to 2-km aperture, which would result in a substantial gain in both long and short period capability.

All of these results rest on an extrapolation of data taken at 10- to 80-second period over spacings of 7 to 60 km. Analysis of more representative data is urgently needed before these conclusions can be accepted as a basis for deployment.

RECOMMENDATIONS FOR FURTHER RESEARCH

As noted above, a high priority must be to determine improved coherence versus distance relations from strong signals in the 0.1- to 3.0-km intersensor distance range. Data should be of signals with good signal-to-noise in order not to confuse loss of signal coherence with random noise.

Data with good signals should soon be available from historical data from Alaska and from the "Windless Bight" station in Antarctica, VNDA. The Alaskan array has sensors separated by intervals of approximately 0.7, 1.4, 1.7, and 2.2 up to 6.2 km while the Antarctic array had sensor spacings of 1, 1.5, and 2.6 up to 6.2 km; both should offer excellent data for analysis. There are on-line arrays in Texas (TXI) and Australia (WRAI). WRAI has elements separated by 0.3, 0.5, and 1.8 to 3 km;, TXI has elements separated by up to 0.3 km.

The above suggests that good signal-to-noise signal waveforms from operational sensors spaced in the critical range of 0.5 to 2 km are likely to continue to be rare for some time from on-line arrays; efforts should be made to modify an existing array or to deploy a temporary array in order to gather the appropriate data for operational testing.

When this data is available the signals could be added at different signal-to-noise ratios to noise from the same sensors, and the actual degradation in azimuth estimates determined by standard processors observed. Also, the errors from subarrays with different apertures could be compared at fixed signal-to-noise.

Processors to implement the optimum detectors and azimuth estimators for uncorrelated signals should be developed and applied to synthetic and actual data. Comparisons could be made to incoherent detectors and azimuth estimators, especially at high frequencies or large apertures where processors which depend on correlation may begin to fail.

REFERENCES

Blandford, R.R. and D. Clauter (1996). Estimation of infrasonic network performance, *AFTAC-TR-97-xxx.*

Blandford, R.R. and D.M. Clark (1975). A note on seismic array design, *Bull. Seism. Soc. Am.*, **65,** 787-791.

Cook, R.K. and A.J. Bedard (1971). On the measurement of infrasound, *Geophys. J. R. astr. Soc.*, **26,** 5-11.

Harris, D.B. (1990). Comparison of the direction estimation performance of high-frequency seismic arrays and three-component stations. *Bull. Seism. Soc. Am.*, **80,** 1951-1968.

Mack, H. and E.A. Flinn (1971). Analysis of the spatial coherence of short-period acoustic-gravity waves in the atmosphere, *Geophys. J. R. astr. Soc.*, **26,** 255-269.

McKisic, M. (1996). Preliminary Draft Report, History of Infrasound Monitoring

Morgan, D.R., and T.M. Smith (1990). Coherence effects on the detection performance of quadratic array processors, with applications to large-array matched-field beamforming, *J. Acoust. Soc. Am.*, **87(2),** 737-747.

McDonald, J.A., E.J. Douze, and E. Herrin (1971). Structure of atmospheric turbulence, *Geophys. J. R. astr. Soc.*, **26,** 99-109.

Olmstead, G.B. (1952). Operations Buster and Jangle, detection of airborne low-frequency sound from the atomic explosions of operations Buster and Jangle, Headquarters US Air Force Office for Atomic Energy, DCS/O AFOAT-1. (Declassified Report)

Whitaker, R.W., J.P. Mutschlecner, M.B. Davidson, and S.D. Noel (1990). Infrasonic observations of large-scale HE events, in *Fourth International Symposium on Long-Range Sound Propagation*, NASA Conference Publication 3101.

Working Group 1 - Verification (1995). International Monitoring System expert group report based on technical discussions held from 6 February to 3 March 1995, *CD/NTB/WP.224.*

Wu, J. (1982). Asymptotic properties of nonlinear least squares estimators in a replicated time series model, *1983 Thesis,* George Washington University, Washington DC

APPENDIX: Detection and Estimation for Propagating Stochastic Signals

Robert H. Shumway
Division of Statistics
University of California, Davis
October 1, 1996

1. The Stochastic Signal Model

In general a model for a collection of signals, observed at an array of N sensors whose response is denoted by $y_j(t), j = 1, \ldots, N, t = 0, 1, \ldots, T-1$ is

$$y_j(t) = s_j\big(t - T_j(\theta)\big) + v_j(t) \tag{1}$$

where $s_j(t)$ are random signals, assumed to be different on each channel, and $T_j(\theta)$ are time delays induced by a propagation pattern indexed by the wavenumber coordinates $\theta = (\theta_1, \theta_2)'$ which are nonlinearly related to the velocity and azimuth of a propagating plane wave. We assume that the signals are stationary processes and denote the $N \times N$ spectral matrix by $f_s(\nu), -.5 \leq \nu \leq .5$. The noise processes are often assumed to be independent and identically distributed across the array but have a stationary correlation structure over time; we denote the common spectral density by $P_n(\nu)$. with ν denoting frequency in cycles per unit time. The time delays are expressed in terms of the physical locations $\mathbf{r}_j = (r_{j1}, r_{j2})'$ of the sensors as

$$T_j(\theta) = \frac{\mathbf{r}_j'\theta}{\nu} \tag{2}$$

over a set of frequencies ν where the assumption (2) can be made. We may also consider a version of (1) which assumes a common stochastic signal, say $s(t)$, on all channels, i.e.

$$y_j(t) = s\big(t - T_j(\theta)\big) + v_j(t), \tag{3}$$

and we refer to this as the *perfect correlation model.*

It is conventional to consider the above model in the frequency at a collection of L frequencies, say $\nu_1, \ldots, \nu_L$ over which the signal and noise spectral matrices are constant, say at f_s and $P_n I_N$ where I_N denotes the $N \times N$ identity matrix. Taking discrete Fourier transforms yields the approximation

$$Y_{j\ell} = A_j(\theta) S_{j\ell} + V_{j\ell} \tag{4}$$

over a set of frequencies $\ell = 1, \ldots, L$, where

$$\begin{aligned} A_j(\theta) &= \exp\{-2\pi i \nu T_j\} \\ &= \exp\{-2\pi i \mathbf{r}_j'\theta\}. \end{aligned} \tag{5}$$

This means that we may write a vector form of (4) in the frequency domain as

$$\mathbf{Y}_\ell = G(\theta)\mathbf{S}_\ell + \mathbf{V}_\ell, \tag{6}$$

where $\mathbf{Y}_\ell, \mathbf{S}_\ell$ and $\mathbf{V}_\ell$ are vector transforms of the observed data, signal and noise respectively and

$$G(\theta) = diag\{A_1(\theta), A_2(\theta), \ldots, A_N(\theta)\} \tag{7}$$

is an $N \times N$ matrix with the $A_j(\theta)'s$ down the diagonal. The spectral matrix of the observed vector $\mathbf{Y}_\ell$ is clearly

$$f_y(\theta) = G(\theta) f_s G^*(\theta) + P_n I_N \tag{8}$$

where C^* denotes the complex conjugate transpose of the matrix C. The mean value of the vector $\mathbf{Y}_\ell$ is zero since the signal and noise processes are assumed to have zero means.

A special case of interest is the perfectly correlated signal where we assume that the model (4) is

$$Y_{j\ell} = A_j(\theta) S_\ell + V_{j\ell}, \tag{9}$$

which is stacked in the form

$$\mathbf{Y}_\ell = \mathbf{g}(\theta) S_\ell + \mathbf{V}_\ell \tag{10}$$

where

$$\mathbf{g}(\theta) = (A_1(\theta), A_2(\theta), \ldots, A_N(\theta))' \tag{11}$$

now becomes an $N \times 1$ vector and the spectral matrix becomes

$$f_y(\theta) = P_s \mathbf{g}(\theta)\mathbf{g}^*(\theta) + P_n I_N. \tag{12}$$

It should be noted that the model discussed in this note differs from the usual case where we regard the signal as being fixed and unknown, but identical between sensors. In that case, the model looks exactly like Equation (9), with the signal assumed to be fixed and unknown. Hence the vector $\mathbf{Y}_\ell$ in this case will have mean $\mathbf{g}(\theta)S - \ell$ and spectral matrix $P_n I_N$. The theory for various proposed estimators in this case has been covered in Hinich and Shaman (1972), Hinich (1981), Wu (1982), Shumway (1983) or Brillinger (1985).

For the stochastic signal case, we consider estimation of the signal and its mean square error in the next section and then move to sections on maximum likelihood detection and estimation in the following sections.

2. Signal Estimation

For the stochastic signal case, it is clear that,in the frequency domain, the signal estimation problem can be solved under either the linearity or Gaussian assumptions by computing the conditional expectation of the signal given the data under the Gaussian assumption. We consider the two cases corresponding to models assuming perfect correlation and more general correlation structures.

2.1 Signal Estimation: The Perfectly Correlated Signal

The perfectly correlated case has also been considered by Harris (1990). Suppose we consider the model given by (9) under the assumptions on the noise and spectral matrices summarized in (11). Using the Gaussian assumptions leads to estimating S_ℓ by

$$\begin{aligned}\hat{S}_\ell(\theta) &= E(S_\ell|\mathbf{Y}_\ell) \\ &= P_s\mathbf{g}^*(\theta)\Big(P_s\mathbf{g}^*(\theta)\mathbf{g}(\theta) + P_nI_N\Big)^{-1}\mathbf{Y}_\ell \\ &= \left(\mathbf{g}(\theta)\mathbf{g}^*(\theta) + \frac{P_n}{P_s}\right)^{-1}\mathbf{g}^*(\theta)\mathbf{Y}_\ell \\ &= \frac{\mathbf{g}^*(\theta)\mathbf{Y}_\ell}{N+r},\end{aligned} \tag{13}$$

where $\mathbf{g}^*(\theta)\mathbf{g}(\theta) = N$ from (5) and (11) and

$$r = \frac{P_n(\nu)}{P_s(\nu)} \tag{14}$$

is the inverse of the signal to noise ratio. The result exhibits the signal estimator as the beam, $\mathbf{g}^*(\theta)\mathbf{Y}_\ell$, adjusted by a multiplier that depends on the number of elements N and the noise to signal ratio r. The mean square error of the signal estimator reduces to

$$\begin{aligned}\sigma^2(\theta) &= P_s - P_s\mathbf{g}^*(\theta)\Big(P_s\mathbf{g}(\theta)\mathbf{g}^*(\theta) + P_nI_N\Big)^{-1}\mathbf{g}(\theta)P_s \\ &= P_n\left(\mathbf{g}^*(\theta)\mathbf{g}(\theta) + \frac{P_n}{P_s}\right)^{-1} \\ &= \frac{P_n}{N+r}.\end{aligned} \tag{15}$$

It is clear that the estimated signal is basically the beamformed estimator $\mathbf{g}^*(\theta)\mathbf{Y}_\ell$ and that the variance of the beam goes down by a factor that is weighted by the number of sensors plus the inverse of the signal to noise ratio.

2.2 Signal Estimation: The General Correlated Signal

For the general stochastic signal case, it is convenient to assume that the transforms are complex Gaussian and again use the fact that the conditional expectation $\hat{\mathbf{S}}_\ell(\theta) = E(\mathbf{S}_\ell|\mathbf{Y}_\ell)$ has the smallest mean square error. For the general model (5), we obtain

$$\begin{aligned}\hat{\mathbf{S}}_\ell(\theta) &= f_sG^*(\theta)\Big(G(\theta)f_sG^*(\theta) + P_nI_N\Big)^{-1}\mathbf{Y}_\ell \\ &= \Big(G^*(\theta)G(\theta) + P_nf_s^{-1}\Big)^{-1}G^*(\theta)\mathbf{Y}_\ell,\end{aligned} \tag{16}$$

using a standard matrix identity (see, for example, Jazwinski, 1970). The estimator involves computing the delayed quantity $A_j(\theta)Y_{j\ell}$ on each sensor and then adjusting by multiplying by the adjustment matrix involving the spectral matrices of the signal and noise. The mean square covariance matrix of the estimator is given by

$$\begin{aligned}\Sigma(\theta) &= f_s - f_s G^*(\theta)\Big(G(\theta)f_s G^*(\theta) + P_n I_N\Big)^{-1} G(\theta) f_s \\ &= P_n\Big(G^*(\theta)G(\theta) + P_n f_s^{-1}\Big)^{-1}, \end{aligned} \tag{17}$$

using another identity from Jazwinski (1970). We note that for $A_j(\theta)$ as defined in (3) and (4), we have the simplification

$$G^*(\theta)G(\theta) = I_N, \tag{18}$$

so that the multiplying matrices in (16) and (17) do not depend on θ, and we may write

$$\hat{\mathbf{S}}_\ell(\theta) = CG^*(\theta)\mathbf{Y}_\ell \tag{19}$$

and

$$\Sigma = P_n C, \tag{20}$$

where

$$C = \Big(I_N + P_n f_s^{-1}\Big)^{-1}, \tag{21}$$

for use in later equations. We notice that the optimal estimator is no longer the beam, but is essentially a weighted beam of the form

$$\hat{S}_{jl}(\theta) = \sum_{k=1}^{N} c_{jk} \exp\{2\pi i \mathbf{r}_k' \theta\} Y_{kl} \tag{22}$$

with weights proportional to the elements of C defined by (21).

3. Maximum Likelihood Estimation

In the stochastic signal case, we regard the wavenumber vector $\theta = (\theta_1, \theta_2)'$ and the nonlinear functions velocity and azimuth, say

$$\begin{aligned} c &= \frac{\nu}{\sqrt{\theta_1^2 + \theta_2^2}} \\ &= \frac{\nu}{\|\theta\|} \end{aligned} \tag{23}$$

and

$$\alpha = \tan^{-1}(\theta_2/\theta_1) \tag{24}$$

as the parameters to be estimated. The log likelihood function is of the form

$$\log L(\theta) = -L \log |f_y(\theta)| - \sum_{\ell=1}^{L} \mathbf{Y}_\ell^* [f_y(\theta)]^{-1} \mathbf{Y}_\ell, \tag{25}$$

where the form taken by the spectral density matrix of the data can be either (8) or (12) depending on whether we have the perfect or general correlation models. Suppose, for the moment, that we only want estimators for the velocity and azimuth. Large sample likelihood theory implies that, for a true value of θ, the distribution of $\hat{\theta}$ is approximately normal with mean θ and covariance matrix

$$cov(\hat{\theta}) = \left\{ -E \frac{\partial^2 \log L(\theta)}{\partial \theta \partial \theta'} \right\}^{-1} \tag{26}$$

Having done this, note that the velocity and azimuth are nonlinear functions, say $\mathbf{h}(\theta) = (c, \alpha)' = (h_1(\theta), h_2(\theta))'$ and the delta method implies that the function is approximately normal with mean $\mathbf{h}(\theta)$ and

$$cov[\mathbf{h}(\hat{\theta})] = \left(\frac{\partial \mathbf{h}}{\partial \theta} \right) cov(\hat{\theta}) \left(\frac{\partial \mathbf{h}}{\partial \theta} \right)' \tag{27}$$

For the velocity and azimuth functions, note that

$$\frac{\partial \mathbf{h}}{\partial \theta} = \frac{1}{\|\theta\|^3} \begin{pmatrix} -\nu\theta_1 & -\nu\theta_2 \\ \\ \|\theta\|\theta_2 & -\|\theta\|\theta_1 \end{pmatrix} \tag{28}$$

The following sections discuss maximum likelihood estimation and derive the limiting distribution of the maximum likelihood estimators for velocity and azimuth. We also derive the likelihood ratio detectors for the signal and its distribution for the perfectly correlated case.

3.1 Maximum Likelihood: The Perfectly Correlated Signal

For the perfectly correlated case, with covariance matrix (11), we may write the log likelihood function (25) as

$$\log L(\theta) = -L \log \frac{P_s}{(N+r)} - \frac{1}{P_n} \sum_{\ell=1}^{L} \mathbf{Y}_\ell^* \mathbf{Y}_\ell + \frac{1}{P_n} \frac{\sum_{\ell=1}^{L} |\mathbf{g}^*(\theta) \mathbf{Y}_\ell|^2}{N+r}. \tag{29}$$

This is seen to be a monotone function of the beam power which will be proportional to

$$B(\theta) = \sum_{\ell=1}^{L} |\mathbf{g}^*(\theta) \mathbf{Y}_\ell|^2. \tag{30}$$

Hence, to maximize the log likelihood, it will be sufficient to maximize the beam power (30) over θ.

Suppose that we look for the likelihood ratio criterion for testing the presence or absence of the signal S_ℓ. Then, for $S_\ell = 0$, we will obtain a test statistic that is a monotone function of the beam power in (30). For any θ, under the hypothesis $P_s = 0$, the distribution of $B(\theta)$ is proportional to a chi-squared distribution with $2L$ degrees of freedom, i.e.

$$\frac{2B(\theta)}{NP_n} \sim \chi^2(2L). \tag{31}$$

Under the alternative hypthesis, assuming the wavenumber vector is evaluated at the correct θ, we have

$$\frac{2B(\theta)}{NP_n} \sim \left(1 + N\frac{P_s}{P_n}\right)\chi^2(2L). \tag{32}$$

If θ_0 is the model value and we use the beam at θ, the distribution of the test statistic is

$$\frac{2B(\theta)}{NP_n} \sim (1 + d(\theta,\theta_0)\frac{P_s}{P_n})\chi^2(2L), \tag{33}$$

where

$$d(\theta,\theta_0) = N^{-1}\sum_{j=1}^{N}\sum_{k=1}^{N}\cos[2\pi(\mathbf{r}_j - \mathbf{r}_k)'(\theta - \theta_0)] \tag{34}$$

and the detection probability is a function of the offset between θ and θ_0.

The uncertainty of the maximum likelihood estimators for velocity and azimuth are evaluated by using (26)-(28) in conjunction with the log likelihood (29) and we note that the covariance matrix of θ simplifies, since

$$\frac{\partial^2 \log L(\theta)}{\partial\theta\partial\theta'} = -\frac{(2\pi)^2}{P_n(N+r)}\sum_{j,k}\sum_{\ell=1}^{L}\exp\{2\pi i(\mathbf{r}_j - \mathbf{r}_k)'\theta\}Y_{j\ell}Y^*_{k\ell}(\mathbf{r}_j - \mathbf{r}_k)(\mathbf{r}_j - \mathbf{r}_k)'.$$

Hence,

$$\begin{aligned} -E\left\{\frac{\partial^2 \log L(\theta)}{\partial\theta\partial\theta'}\right\} &= (2\pi)^2\frac{L}{(N+r)}\frac{P_s}{P_n}\sum_{j,k}(\mathbf{r}_j\mathbf{r}_j' - \mathbf{r}_j\mathbf{r}_k' - \mathbf{r}_k\mathbf{r}_j' + \mathbf{r}_k\mathbf{r}_k') \\ &= \frac{2(2\pi)^2N^2L}{r(N+r)}\,R, \end{aligned} \tag{35}$$

where

$$R = \frac{1}{N}\sum_{j=1}^{N}(\mathbf{r}_j - \bar{\mathbf{r}})(\mathbf{r}_j - \bar{\mathbf{r}})' \tag{36}$$

is the sample covariance matrix of the array coordinates. It follows that $\hat{\theta}$ will be approximately normal with mean θ and approximate covariance matrix

$$cov(\hat{\theta}) \approx \frac{1}{2(2\pi)^2}\frac{1}{L}\frac{r}{N}\left(1+\frac{r}{N}\right)R^{-1} \tag{37}$$

where r is the inverse of the signal-to-noise ratio (13). Then, defining the vectors $\theta = (\theta_1, \theta_2)'$ and $\tilde{\theta} = (\theta_2, -\theta_1)'$, we obtain the variance estimators for

$$var\ \hat{c} \approx \frac{1}{2(2\pi)^2}\frac{r}{N}\left(1+\frac{r}{N}\right)\frac{\nu^2}{\|\theta\|^6}\frac{\theta' R^{-1}\theta}{L} \tag{38}$$

and

$$var\ \hat{\alpha} \approx \frac{1}{2(2\pi)^2}\frac{r}{N}\left(1+\frac{r}{N}\right)\frac{1}{\|\theta\|^4}\frac{\tilde{\theta}' R^{-1}\tilde{\theta}}{L}. \tag{39}$$

Evaluating the above equations at $\hat{\theta}$ will produce consistent estimators for the variances.

3.2 Maximum Likelihood: The General Correlated Signal

For the signal with a general correlation structure, as in (1), the log likelihood has the covariance structure given by (7) and we write (24) in the form

$$\begin{aligned}\log L(\theta) \propto & -L\log|f_s| - \log|I_N + P_n f_s^{-1}| \\ & - \frac{1}{P_n}\sum_{\ell}\mathbf{Y}_\ell^*\mathbf{Y}_\ell + \frac{1}{P_n}\sum_{l}\mathbf{Y}_\ell^* G(\theta)\left(I_N + P_n f_s^{-1}\right)^{-1} G^*(\theta)\mathbf{Y}_\ell.\end{aligned} \tag{40}$$

Then, noting that the Hermitian form contains the matrix C in (21), we may write the likelihood ratio detector in the form

$$\tilde{B}(\theta) = \frac{1}{P_n}\sum_{\ell=1}^{L}\hat{\mathbf{S}}_\ell^*(\theta)C^{-1}\hat{\mathbf{S}}_\ell(\theta) \tag{41}$$

using (18). The form (41) makes it easy to infer the distribution, since each term is distributed as a chi-square with 2 degrees of freedom, conditionally on $Y_\ell, \ell = 1, \ldots, L$. Hence the unconditional distribution of $\tilde{B}(\theta)$ is again proportional to a chi-squared distribution with $2L$ degrees of freedom.

We may derive variance formulae using an argument similar to that for the perfectly correlated case. First, note that

$$\begin{aligned}\frac{\partial^2 \log L(\theta)}{\partial\theta\partial\theta'} &= \frac{\partial^2}{\partial\theta\partial\theta'}\left\{\frac{1}{P_n}\sum_{\ell=1}^{L}\mathbf{Y}_\ell^* G(\theta)CG(\theta)\mathbf{Y}_\ell\right\} \\ &= \frac{\partial^2}{\partial\theta\partial\theta'}\left\{\frac{1}{P_n}\sum_{j,k}\sum_{\ell}Y_{j\ell}^* Y_{k\ell}c_{jk}\exp\{-2\pi i(\mathbf{r}_j - \mathbf{r}_k)'\theta\}\right\} \\ &= -(2\pi)^2\frac{1}{P_n}\sum_{j,k}\sum_{\ell}c_{jk}Y_{j\ell}^* Y_{k\ell}(\mathbf{r}_j - \mathbf{r}_k)(\mathbf{r}_j - \mathbf{r}_k)'\exp\{-2\pi i(\mathbf{r}_j - \mathbf{r}_k)'\theta\}.\end{aligned}$$

Taking expectations, we obtain

$$-E\left\{\frac{\partial^2 \log L(\theta)}{\partial\theta\partial\theta'}\right\} = (2\pi)^2 \frac{L}{P_n} \sum_{j,k} c_{jk} f^s_{kj} (\mathbf{r}_j - \mathbf{r}_k)(\mathbf{r}_j - \mathbf{r}_k)'$$

$$= (2\pi)^2 \frac{L}{P_n} D, \tag{42}$$

where f^s_{jk} denotes the jk^{th} element of the signal spectral matrix and

$$D = \sum_{j,k} c_{jk} f^s_{kj} (\mathbf{r}_j - \mathbf{r}_k)(\mathbf{r}_j - \mathbf{r}_k).' \tag{43}$$

In this case we will have $\hat{\theta}$ distributed approximately as a normal random variable with mean θ_0 and covariance matrix

$$cov\ \hat{\theta} \approx \frac{1}{(2\pi)^2} \frac{P_n}{L} D^{-1} \tag{44}$$

leading to estimated variances for the velocity and azimuth of the form

$$var\ \hat{c} \approx \frac{1}{(2\pi)^2} P_n \frac{\nu^2}{\|\theta\|^6} \frac{\theta' D^{-1} \theta}{L} \tag{45}$$

and

$$var\ \hat{\alpha} \approx \frac{1}{(2\pi)^2} P_n \frac{1}{\|\theta\|^4} \frac{\tilde{\theta}' D^{-1} \tilde{\theta}}{L} \tag{46}$$

REFERENCES

Brillinger, D.R. (1985). A maximum likelihood approach to frequency-wavenumber analysis. *IEEE Trans. on Acoustics, Speech and Signal Processing* **33** 1076-1085.

Capon, J. (1969). High resolution frequency wavenumber spectrum analysis. *Proc. IEEE* **57** 1408-1418.

Harris, D. B. (1990) Comparison of the direction estimation performance of high-frequency seismic arrays and three- component stations. *Bull. Seismolog. Soc. Amer.* **80** 1951-1968.

Hinich, M.J. (1981). Frequency-wavenumber array processing. *J. Acoust. Soc. Amer.* **69** 732-737.

Hinich, M.J. and P. Shaman (1972). Parameter estimation for an R-dimensional plane wave observed with additive independent Gaussian errors. *Ann. Math. Statist.* **43** 153-169.

Jazwinski, A.H. (1970). *Stochastic Processes and Filtering Theory.* Appendix 7B, pp. 261-262. New York: Academic Press

Shumway, R.H. (1983). Replicated time series regression: An approach to signal estimation and detection. In Brillinger, Krishnaiah ed. *Handbook of Statistics, Vol. 3, Time Series in the Frequency Domain* Amsterdam: North Holland.

Wu, J. S-H (1982). Asymptotic properties of nonlinear least squares estimators in a replicated time series model. (1982). Ph.D. Dissertation, The George Washington University, Washington, D.C.

DISTRIBUTION

California Institute of Technology
ATTN: Prof. Thomas Ahrens
Seismological Laboratory, 252-21
Pasadena CA 91125

Air Force Research Laboratory
ATTN: Research Library/TL
5 Wright St.
Hanscom AFB MA 01731-3004

Air Force Research Laboratory
ATTN: VSOE
29 Randolph Rd.
Hanscom AFB MA 01731-3010

Air Force Research Laboratory
ATTN: AFRL/SUL
3550 Aberdeen Ave., SE
Kirtland AFB NM 87117-5776

NTPO
ATTN: Dr. R.W. Alewine
1901 N. Moore Street, Suite 609
Arlington VA 22209

Pennsylvania State University
ATTN: Prof. S. Alexander &
Prof. C.A. Langston
Department of Geosciences
537 Deike Building
University Park PA 16802

University of Colorado
ATTN: Prof. C. Archambeau, Prof. D. Harvey,
Dr. Anatoli Levshin, & Prof. M. Ritzwoller
Department of Physics
Campus Box 583
Boulder CO 80309-0583

Science Application International Corporation
ATTN: Dr. T. Bache, Jr. & Dr. T.J. Sereno
10260 Campus Point Drive
San Diego CA 92121-1578

Center for Monitoring Research
ATTN: Librarian
1300 N. 17th St., Suite 1450
Arlington VA 22209

Cornell University
ATTN: Prof. M. Barazangi
Institute for the Study of the Continents
Department of Geological Sciences
3126 SNEE Hall
Ithaca NY 14853

State University of New York, Binghamton
ATTN: Prof. F.T. Wu
Department of Geological Sciences
Binghamton NY 13901

Maxwell Technologies
ATTN: Dr. T.G. Barker & Dr. J. Stevens
8888 Balboa Ave.
San Diego CA 92123-1506

ENSCO, Inc./APA Division
ATTN: Dr. D.R. Baumgardt & Dr. Z. Der
5400 Port Royal Road
Springfield VA 22151-2388

University of Arizona
ATTN: Dr. S. Beck & Prof. T.C. Wallace
Department of Geosciences
Gould Simpson Building
Tuscon AZ 85721

Maxwell Technologies
ATTN: Dr. T.J. Bennett & Mr. J. Murphy
Geophysics & Resource Technologies Group
11800 Sunrise Valley Drive, Suite 1212
Reston VA 22091

University of California, San Diego
ATTN: Dr. J. Berger, Dr. L. Burdick, Dr. H.
Given, Dr. M. Hedlin, Prof. B. Minster,
Prof. J.A. Orcutt, & Dr. F.L. Vernon
Scripps Institution of Oceanography
IGPP, 0225
9500 Gilman Dr.
La Jolla CA 92093-0255

Schlumberger-Doll Research Center
ATTN: Dr. R. Burridge
Old Quarry Road
Ridgefield CT 06877

Department of Energy
ATTN: Ms. Leslie A. Casey
Office of R&D, NN-20
1000 Independence Ave., SW
Washington DC 20585-0420

Virginia Polytechnical Institute
ATTN: Dr. M. Chapman
Seismological Observatory
Department of Geological Sciences
4044 Derring Hall
Blacksburg VA 24061-0420

Arms Control & Disarmament Agency
ACDA/IVI/VC
ATTN: Mr. R. Cockerham & Mr. R. Morrow
320 21st Street N.W.
Washington DC 20451

University of Connecticut, Storrs
ATTN: Prof. V.F. Cormier
Department of Geology & Geophysics
U-45, Room 207
Storrs CT 06269-2045

HQ DSWA/PMA
ATTN: Dr. Anton Dainty
6801 Telegraph Rd.
Alexandria VA 22310-3398

San Diego State University
ATTN: Dr. S. Day
Department of Geological Sciences
San Diego CA 92182

Defense Technical Information Center
8725 John J. Kingman Road, Suite 0944
Ft. Belvoir VA 22060-6218

University of California, San Diego
ATTN: Dr. Catherine de Groot-Hedlin
Institute of Geophysics & Planetary Sciences
8604 La Jolla Shores Drive
San Diego CA 92093

University of Texas, El Paso
ATTN: Ms. Diane Doser
Department of Geological Sciences
El Paso TX 79968

Harvard University
ATTN: Prof. A. Dziewonski
Hoffman Laboratory
Department of Earth, Atmospheric &
Planetary Sciences
20 Oxford Street
Cambridge MA 02138

Boston College
ATTN: Prof. J. Ebel & Prof. A. Kafka
Department of Geology & Geophysics
Chestnut Hill MA 02167

Mission Research Corporation
ATTN: Dr. M. Fisk & Dr. W. Wortman
8560 Cinderbed Rd., Suite 700
Newington VA 22122

Brown University
ATTN: Prof. D. Forsyth
Department of Geological Sciences
Providence RI 02912

Defense Intelligence Agency/PAG-1A
ATTN: Dr. D.P. Glover
Washington DC 20340-6160

Multimax, Inc.
ATTN: Ms. Lori Grant
311C Forest Ave., Suite 3
Pacific Grove CA 93950

Southern Methodist University
ATTN: Dr. Henry Gray
Department of Statistics
P.O. Box 750302
Dallas TX 75275-0302

Multimax, Inc.
ATTN: Dr. I.N. Gupta & Mr. W. Rivers
1441 McCormick Drive
Largo MD 20774

Pacific Northwest National Laboratories
ATTN: Mr. D.N. Hagedorn
P.O. Box 999, MS F5-12
Richland WA 99352

Lawrence Livermore National Laboratory
ATTN: Dr. J. Hannon & Dr. K. Nakanishi
P.O. Box 808, L-205
Livermore CA 94550

MIT ERL E34-404
ATTN: Dr. David Harkrider
42 Carlton St.
Cambridge MA 02142-1324

New Mexico State University
ATTN: Prof. Thomas Hearn & Prof. James Ni
Department of Physics
Las Cruces NM 88003

California Institute of Technology
ATTN: Dr. Donald Helmberger
Division of Geological & Planetary Sciences
Seismological Laboratory
Pasadena CA 91125

Southern Methodist University
ATTN: Dr. E. Herrin & Dr. B. Stump
Department of Geological Sciences
P.O. Box 750395
Dallas TX 75275-0395

St. Louis University
ATTN: Prof. R. Herrmann & Prof. B. Mitchell
Department of Earth & Atmospheric Sciences
3507 Laclede Ave.
St. Louis MO 63103

HQ DSWA/PMP/CTBT
ATTN: Dr. M. Shore & Mr. Rong-Song Jih
6801 Telegraph Rd.
Alexandria VA 22310-3398

University of California, Berkeley
ATTN: Prof. L.R. Johnson &
Prof. T. McEvilly
Earth Sciences Division
LBNL 90-2106, MS 90-1116
479 McCone Hall
Berkeley CA 94720

Massachusetts Institute of Technology
ATTN: Prof. T.H. Jordan
Department of Earth, Atmospheric &
Planetary Sciences
77 Massachusetts Ave., 654-918
Cambridge MA 02139

Massachusetts Institute of Technology
ATTN: Dr. R. LaCross, M-200B
Lincoln Laboratory
P.O. Box 73
Lexington MA 02173-0073

University of Illinois, Urbana-Champaign
ATTN: Prof. F.K. Lamb & Prof. J. Sullivan
Department of Physics
1110 West Green Street
Urbana IL 61801

Oklahoma Geological Survey Observatory
ATTN: Dr. J. Lawson, Chief Geophysicist
P.O. Box 8
Leonard OK 74043-0008

University of California, Santa Cruz
ATTN: Dr. T. Lay, Dr. S. Schwartz, & Dr. R. Wu
Earth Sciences Dept.
Earth & Marine Sciences Building
Santa Cruz CA 95064

US Geological Survey
ATTN: Dr. W. Leith
920 National Center
Reston VA 22092

Weston Geophysical Corp.
ATTN: Mr. James Lewkowicz
325 West Main St.
Northboro MA 01532

ACDA/VI-OA
ATTN: Mr. A Lieberman
State Department Building, Room 5726
320 21st Street, NW
Washington DC 20451

AFTAC/CA(STINFO)/TT/TTR/TTD
1030 South Highway A1A
Patrick AFB FL 32925-3002

Georgia Institute of Technology
ATTN: Prof. L.T. Long
School of Geophysical Sciences
Atlanta G 30332

US Geological Survey
ATTN: Dr. R. Masse
Denver Federal Building
Box 25046, Mail Stop 907
Denver CO 80225

Southern Methodist University
ATTN: Dr. G. McCartor
Department of Physics
P.O. Box 750175
Dallas TX 75275-0175

US Geological Survey
ATTN: Dr. A. McGarr
National Earthquake Center
345 Middlefield Rd., MS-977
Menlo Park CA 94025

Center for Monitoring Research
ATTN: Dr. K.L. McLaughlin & Dr. R. North
1300 North 17th Street
Arlington VA 22209-3871

Office of the Secretary of Defense
DDR&E
Washington DC 20330

Yale University
ATTN: Prof. J. Park
Department of Geology & Geophysics
P.O. Box 208109
New Haven CT 06520-8109

University of Cambridge
ATTN: Prof. Keith Priestly
Bullard Labs, Department of Earth Sciences
Madingley Rise, Madingley Road
Cambridge CB3 OEZ, UNITED KINGDOM

BBN Systems & Technologies
ATTN: Dr. J.J. Pulli
1300 N. 17th St., Suite 1200
Arlington VA 22209

Defense Special Weapons Agency
ATTN: Dr. R. Reinke, FCDNA/FCTTS
1680 Texas S., SE
Kirtland AFB NM 87117-5669

DTR Associates
ATTN: Dr. Delaine Reiter
73 Standish Rd.
Watertown MA 02172

Columbia University
ATTN: Prof. P. Richards & Dr. J. Xie
Lamont-Doherty Geological Observatory
Route 9W
Palisades NY 10964

Woodward-Clyde Federal Services
ATTN: Dr. C.K. Saikia
566 El Dorado Street, Suite 100
Pasadena CA 91101-2560

University of Southern California, Los Angeles
ATTN: Prof. C.G. Sammis
Center for Earth Sciences
University Park
Los Angeles CA 90089-0741

Secretary of the Air Force
(SAFRD)
Washington DC 20330

University of California, Davis
ATTN: Dr. R. Shumway
Division of Statistics
410 MRAK Hall
Davis CA 95616-8671

IRIS
ATTN: Prof. D. Simpson & Dr. G. van der Vink
1616 N. Fort Myer Dr., Suite 1050
Arlington VA 22209

AFOSR/NL
110 Duncan Avenue
Bolling AFB
Washington DC 20332-0001

Los Alamos National Laboratory
ATTN: Dr. H. Patton, Dr. S.R. Taylor,
Dr. Jill Warren, & Dr. T. Weaver
Geophysics Group EES-3, MS C335
P.O. Box 1663
Los Alamos NM 87545

Massachusetts Institute of Technology
ATTN: Prof. M.N. Toksoz
Earth Resources Lab, 34-440
42 Carleton Street
Cambridge MA 02142

ACIS
ATTN: Dr. L. Turnbull
New Headquarters Bldg., Room 4W03
Washington DC 20505

National Science Foundation
ATTN: Dr. Daniel Weill
Division of Earth Sciences, EAR-785
4201 Wilson Blvd., Room 785
Arlington VA 22230

I.R.I.G.M. - B.P. 68
ATTN: Dr. Michel Bouchon
38402 St. Martin D'Heres
Cedex, FRANCE

I.R.I.G.M. - B.P. 53
ATTN: Dr. Michel Campillo
Observatorie de Grenoble
38041 Grenoble, FRANCE

University of Toronto
ATTN: Dr. Kin Yip Chun
Physics Department
Geophysics Division
Ontario, M5S 1A7, CANADA

Ruhr University, Bochum
ATTN: Prof. Hans-Peter Harjes &
Dr. Johannes Schweitzer
Institute for Geophysics
P.O. Box 102148
W-4630 Bochum 1, GERMANY

NTNF/NORSAR
ATTN: Dr. Svein Mykkeltveit
P.O. Box 51
N-2007 Kjeller, NORWAY

Bureau of Mineral Resources
ATTN: Mr. David Jepsen, Acting Head,
Nuclear Monitoring Section
Geology and Geophysics
G.P.O. Box 378
Canberra, ACT 2601, AUSTRALIA

National Defense Research Institute
ATTN: Ms. E. Johannisson
Senior Research Officer
P.O. Box 27322
S-102 54 Stockholm, SWEDEN

Atomic Weapons Establishment
ATTN: Dr. P. Marshall
Blacknest, Brimpton
Reading FG7 4RS, UNITED KINGDOM

Societe Radiomana
ATTN: Dr. Bernard Massinon &
Dr. Pierre Mechler
27 rue Claude Bernard
75005 Paris, FRANCE

University of Bergen
ATTN: Prof. Eystein Husebye
Institute for Solid Earth Physics
Allegaten 40
N-5007, Bergen, NORWAY